Robotica (2025), **43**, pp. 3755–3781
doi:10.1017/S0263574725102671

CAMBRIDGE UNIVERSITY PRESS

RESEARCH ARTICLE

Interactive mechatronic system for improving upper limb rehabilitation

Simone Leone[1], Med Amine Laribi[2], Eduardo Castillo-Castaneda[3] and Giuseppe Carbone[1]

[1]Department of Mechanical, Energy and Management Engineering, University of Calabria - Rende, Rende, Italy
[2]Department of GMSC, Pprime Institute CNRS, ENSMA, UPR 3346, University of Poitiers, Poitiers, France
[3]CICATA-Unidad Querétaro, Instituto Politécnico Nacional, Querétaro, México
Corresponding author: Simone Leone; Email: simone.leone@unical.it

Received: 24 February 2025; **Revised:** 13 July 2025; **Accepted:** 20 September 2025; **First published online:** 17 October 2025

Keywords: robotic rehabilitation technology; upper limb rehabilitation; variable stiffness device; VSJ; VSA; customisable rehabilitation; interactive rehabilitation; real-time adaptability; modular design

Abstract

This study presents an innovative system for upper limb rehabilitation, combining a variable stiffness device, the ReHArm prototype, with a dynamic and engaging user interface, known as Arms Rehabilitation Management System. The proposed system offers a highly customisable approach to rehabilitation, ensuring real-time adaptability to patients' specific needs while maintaining compactness and ease of use. Key features include a modular design allowing precise stiffness adjustments, a robust control architecture, and interactive rehabilitation phases designed to enhance user engagement. Extensive multidisciplinary analyses, including kinematic, dynamic, and structural evaluations, demonstrate the system's ability to improve therapy effectiveness through tailored interaction and feedback. Validation tests demonstrated the prototype's reliability and robustness, and initial usability assessments suggest its potential to improve rehabilitation outcomes. Further clinical studies involving patients will be necessary to fully evaluate its therapeutic effectiveness.

1. Introduction

More than a billion people worldwide live with some form of disability, with nearly 200 million experiencing functional limitations of the upper limbs, a number increasing due to ageing and chronic conditions [1]. In 2019, 20.3% of the EU population was over 65, correlating with increased motor disabilities and musculoskeletal or neurological disorders [2]. These conditions critically impact quality of life by limiting activities of daily living (ADL) and restricting upper limb range of motion (ROM) [3, 4].

The upper limbs are essential for many activities but can be affected by diseases or injuries that impair their mobility and functionality. Their rehabilitation is therefore crucial and increasingly important in the medical and social fields, both due to their complex articulation and the essential functions they perform [5]. An effective rehabilitation programme helps patients regain function and independence, enhancing strength, coordination, and quality of life [5], through targeted protocols featuring repetitive exercises designed to improve muscle tone, range, and precision of movement [6]. The therapist's goal is to develop a rehabilitation plan based on the patient's clinical condition and functional level, engaging him in specific exercises and movements to promote recovery (active rehabilitation) or applying therapies and treatments without the patient's active participation (passive rehabilitation) [7].

Robotics has made significant progress in upper limb rehabilitation, introducing solutions capable of optimising treatment effectiveness, allowing a high level of personalisation, and supporting therapists in real-time progress monitoring, facilitating adjustments to the rehabilitation plan [8, 9]. These devices

© The Author(s), 2025. Published by Cambridge University Press. This is an Open Access article, distributed under the terms of the Creative Commons Attribution licence (https://creativecommons.org/licenses/by/4.0/), which permits unrestricted re-use, distribution and reproduction, provided the original article is properly cited.

https://doi.org/10.1017/S0263574725102671 Published online by Cambridge University Press

are divided into exoskeletons, which adapt to the body to allow precise joint movements [10], and end effectors, which act on the distal part of the limb with a simpler structure and control [11].

In recent years, rehabilitation devices have integrated variable stiffness joints (VSJ) and variable stiffness actuators (VSA) to modulate stiffness according to the patient's needs and the task performed [12]. VSJs regulate resistance to movement in real time, increasing stiffness under high loads and reducing it to mitigate impacts [12]. Depending on their configuration, they can modulate stiffness through serial systems, which adjust internal components [13, 14]; antagonistic systems, based on the interaction of opposing elements [15]; or hybrid systems that combine both approaches. The main methods involve the use of springs [16], fluids [17], smart materials [18, 19], magnets [20], or granular materials [21], each offering advantages and limitations in terms of precision, complexity, and cost [22]. VSAs, on the other hand, dynamically adjust stiffness in response to external stimuli, replicating human muscle flexibility [13] and enhancing interaction, energy efficiency, and rehabilitation applications [15, 23]. These devices may also rely on smart materials [24], transmission mechanisms [25, 26], or fluids [27], each providing specific benefits in terms of precision, robustness, and performance depending on the application. The combination of these technologies in rehabilitation devices has proven effective, allowing for targeted adaptability during therapy. Furthermore, integration with user interfaces optimises treatment by allowing precise control and real-time feedback monitoring [28], improving musculoskeletal function, flexibility, and safety, as well as adherence to therapy [29]. Examples include Hand of Hope [30], which employs VSJ for adaptive resistance in hand rehabilitation; ARMEO Spring [31], which uses a spring-based system; and MIT-Manus [32] and ReoGo [33], which use VSA for adaptive support and monitoring interfaces. Other devices, such as RoboTherapist [34] and ArmAssist [35], combine VSJ and VSA for personalised upper limb rehabilitation. Despite the advances these systems have brought, they often have limitations in at least one of the following areas: dynamic stiffness modulation, modular hardware design, or interactivity of the user interface. Systems such as Hand of Hope and ARMEO Spring [30, 31], although widely adopted, rely on predefined stiffness adjustment mechanisms that lack real-time responsiveness or versatility across different phases of rehabilitation. Similarly, MIT-Manus and ReoGo [32, 33] provide adaptive support but offer limited user engagement due to their minimal interactive interfaces. Devices such as RoboTherapist and ArmAssist [34, 35], which combine VSJ and VSA technologies, have demonstrated their potential in personalised rehabilitation but still have limitations in terms of modularity, home usability, and real-time adaptability of their control architectures.

In this context, the following work presents an innovative system for upper limb rehabilitation, which stands out from the currently available solutions for the integration of advanced technologies and a highly customisable therapeutic approach. The system is composed of the ReHArm prototype device, based on a compact VSJ-VSA mechanism capable of modulating stiffness in real time in response to sensory input, and the A.R.M.S. (Arms Rehabilitation Management System) user interface, as illustrated in Figure 1. Compared to conventional devices, the ReHArm features a modular and ergonomic design that allows its use both in clinical and home settings, while the A.R.M.S. interface is designed to improve patient-device interaction through gamified feedback and structured therapeutic progressions. This combination allows for custom treatment and promotes greater patient involvement, allowing the therapist to create individual profiles, monitor the progress of sessions, and adapt therapy parameters in real time according to the specific needs of the individual user. The article provides an in-depth analysis of the developed system, starting from the multidisciplinary technical analysis conducted, describing its overall architecture, which integrates the ReHArm prototype variable stiffness device, the A.R.M.S. user interface, and the implemented control logic, through to the experimental evaluation by means of standardised tests. A preliminary version of this work was presented at the 5th International Conference IFToMM ITALIA – IFIT 2024 [8].

2. Multidisciplinary analysis and simulations

This section presents a multidisciplinary analysis of the device, integrating kinematic and dynamic studies to evaluate motion, operating forces, and workspace requirements, in order to understand the interactions between components and ensure a reliable response under variable conditions.

https://doi.org/10.1017/S0263574725102671 Published online by Cambridge University Press



Figure 1. *The design of the proposed system: ReHArm prototype and A.R.M.S. interface.*

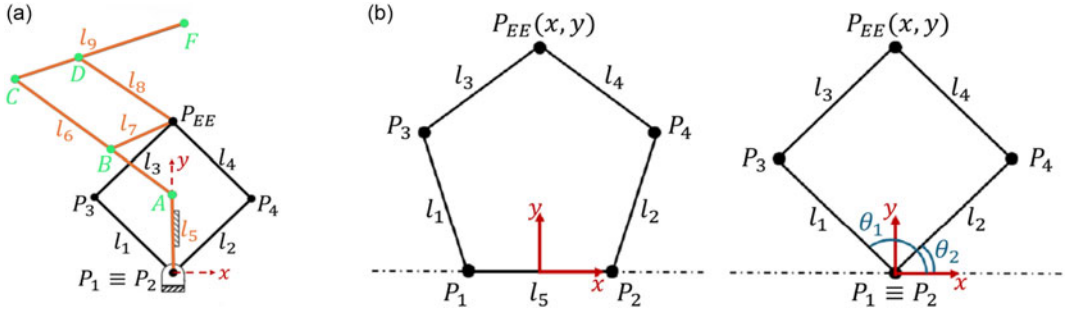


Figure 2. *Schematisation of the device: (a) full configuration; (b) simplified schematic representation.*

2.1. Forward and inverse kinematic analysis

To study forward and inverse kinematics, according to the literature [36, 37], the device was schematised as visible in Figure 2. In particular, since the position of the end effector is provided by Cartesian coordinates (X,Y) and the working area is planar, as well as the 5-bar mechanism, two degrees of freedom are sufficient to characterise its control, that is, only the two active joints (θ_1, θ_2).

Based on the simplified model, it is possible to determine the coordinates P_3 and P_4 in terms of active joints and link lengths (given by the relationship $l_1 = l_2 = l_3 = l_4$, see Figure 2b) together with the constraint equation defining their distance:

$$P_3 = \left[l_1 \cos(\theta_1)\ l_1 \sin(\theta_1)\right]^T, \quad P_4 = \left[l_2 \cos(\theta_2)\ l_2 \sin(\theta_2)\right]^T \tag{1}$$

This gives the distance relationship:

$$\|PP_i\| = L_i, \quad \text{where} \quad i = 3, 4 \tag{2}$$

The explicit form of the equation can be written as:

$$(x - l\cos(\theta_1))^2 + (y - l\sin(\theta_1))^2 = l^2, \quad (x - l\cos(\theta_2))^2 + (y - l\sin(\theta_2))^2 = l^2 \tag{3}$$

To solve the forward kinematics problem, both equations are expanded and subtracted, leading to:

$$x = \frac{l\sin(\theta_1 - \theta_2)(\sin(\theta_1) - \sin(\theta_2))}{1 - \cos(\theta_1 - \theta_2)}, \quad y = \frac{l\sin(\theta_1 - \theta_2)(\cos(\theta_2) - \cos(\theta_1))}{1 - \cos(\theta_1 - \theta_2)} \tag{4}$$

For the inverse kinematics problem, since the equations are identical except for the angles, they can be written in matrix form where the joint angles θ_1 and θ_2 satisfy:

$$A\cos(\theta_i) + B\sin(\theta_i) = C \tag{5}$$

https://doi.org/10.1017/S0263574725102671 Published online by Cambridge University Press

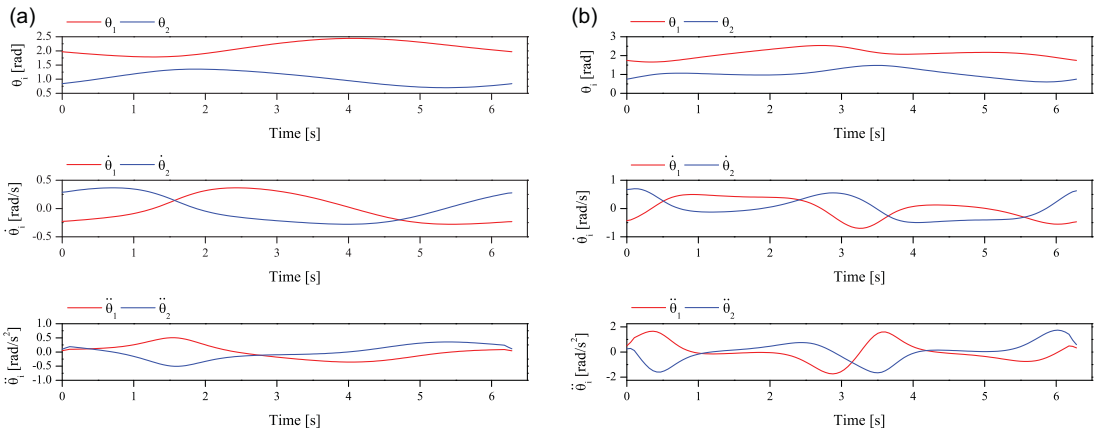


Figure 3. *Theoretical results for positions, velocities, and accelerations: (a) circular trajectory; (b) figure-eight trajectory. The values of θ_1 are shown in red, while those of θ_2 are in blue.*

where variables are defined as: $A = 2xl$, $B = 2yl$, and $C = x^2 + y^2$. Dividing both sides by $\sqrt{A^2 + B^2} = 2l\sqrt{x^2 + y^2}$, we can rewrite the equation as:

$$\cos(\gamma)\cos(\theta_i) + \sin(\gamma)\sin(\theta_i) = \frac{x^2 + y^2}{2l\sqrt{x^2 + y^2}} \quad \text{where} \quad \gamma = \operatorname{atan2}\left(\frac{x}{\sqrt{x^2 + y^2}}, \frac{y}{\sqrt{x^2 + y^2}}\right) \tag{6}$$

Using the trigonometric addition identity, the inverse kinematics problem can be solved to determine the joint angles θ_1 and θ_2:

$$\cos(\gamma - \theta_i) = \frac{x^2 + y^2}{2l\sqrt{x^2 + y^2}} \quad \Rightarrow \quad \theta_i = \gamma \pm \cos^{-1}\left(\frac{x^2 + y^2}{2l\sqrt{x^2 + y^2}}\right) \tag{7}$$

Figure 3 shows the theoretical position, velocity, and acceleration results for the circular and figure-of-eight implemented trajectories, with the angle values θ_1 in red and those of θ_2 in blue.

2.2. Study of workspace and manoeuvring capabilities

The average anthropometric parameters were used to calculate the workspace required for the upper limb rehabilitation movements, according to the literature [36, 37]. The average arm length from the shoulder to the centre of the hand was estimated to be 667.5 mm, resulting in a planar working space of 700 × 1400 mm. Considering the limit of movement of the main joints of the 5-bar mechanism [0°−180°], the links ratio and the amplification factor of 4 given by the pantograph, the length of the links needed to cover the entire working space results:

$$\sum_{i=1}^{n} l_i = 720\ \text{mm} \implies l_i = \frac{720}{4} = 180\ \text{mm} \tag{8}$$

This allowed us to determine the workspace and the dexterity space (Figure 4), where the trajectories are coloured red to confirm that they are fully contained.

2.3. Dynamic analysis and control parameters

After deriving the kinematics models for the 5-bar mechanism, the next step is to determine the Jacobian matrix required to analyse the mechanism's dynamics. Differentiating the equations in (4) with respect to time, considering that $\theta_i = \theta_1, \theta_2$ and x, y, θ_i are functions of time t, we obtain:

$$l\left[y\cos(\theta_i) - x\sin(\theta_i)\right]\dot{\theta}_i = \left[x - l\cos(\theta_i)\right]\dot{x} + \left[y - l\sin(\theta_i)\right]\dot{y} \tag{9}$$

https://doi.org/10.1017/S0263574725102671 Published online by Cambridge University Press

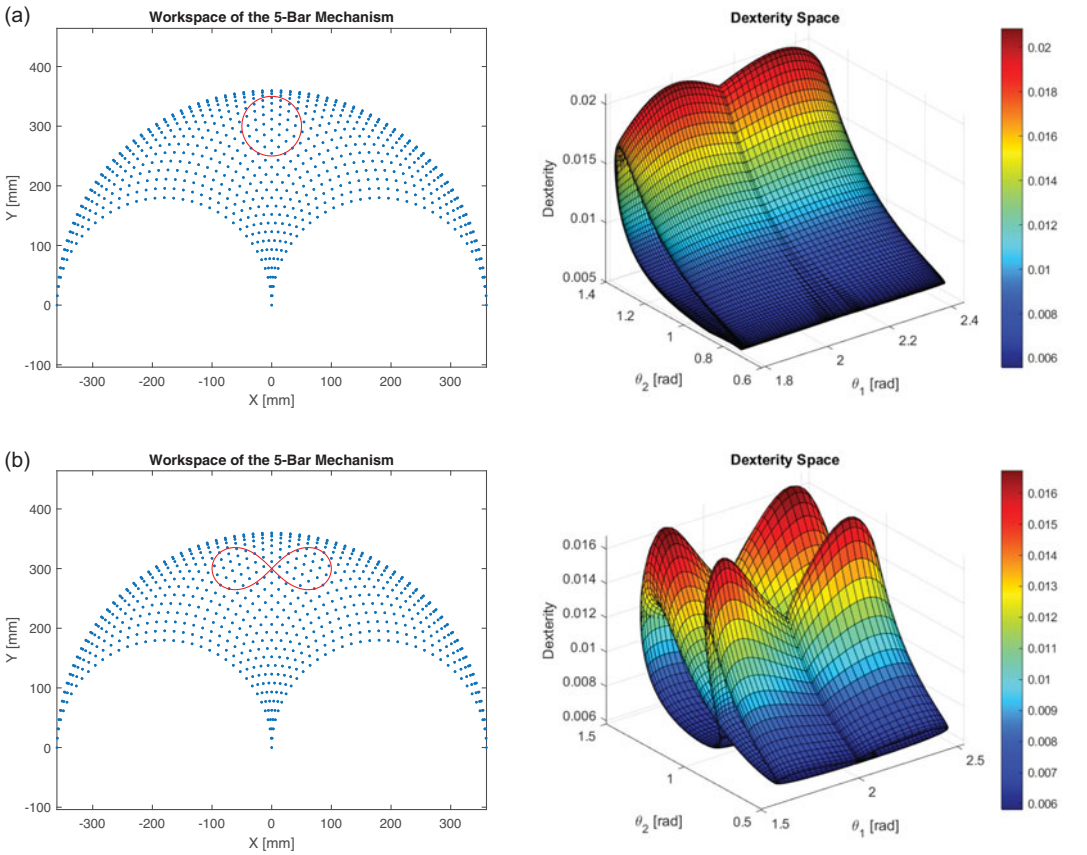


Figure 4. *Workspace and dexterity space: (a) circular trajectory; (b) figure-eight trajectory.*

Considering that $\dot{P} = (\dot{x}, \dot{y})^T$ and $\dot{\theta} = (\dot{\theta}_1, \dot{\theta}_2)^T$ are the output and input velocity vectors, defining $s_i = \sin(\theta_i)$ and $c_i = \cos(\theta_i)$ (for $i = 1, 2$), we can rewrite the equation in matrix form:

$$A\dot{\theta} = B\dot{P} \quad \Rightarrow \quad l \begin{bmatrix} (yc_1 - xs_1) & 0 \\ 0 & (yc_2 - xs_2) \end{bmatrix} \begin{bmatrix} \dot{\theta}_1 \\ \dot{\theta}_2 \end{bmatrix} = \begin{bmatrix} (x - lc_1)\ (y - ls_1) \\ (x - lc_2)\ (y - ls_2) \end{bmatrix} \begin{bmatrix} \dot{x} \\ \dot{y} \end{bmatrix} \tag{10}$$

Thus, the Jacobian matrix is:

$$J = A^{-1}B = \frac{1}{\det(A)} l \begin{bmatrix} (yc_2 - xs_2) & 0 \\ 0 & (yc_1 - xs_1) \end{bmatrix} \begin{bmatrix} (x - lc_1)\ (y - ls_1) \\ (x - lc_2)\ (y - ls_2) \end{bmatrix} \tag{11}$$

So, the required torque τ as a function of the desired position change Δx can be calculated as:

$$\tau = J^T F = J^T k \Delta x \tag{12}$$

The simulation results provided force and torque values for the circular (Figure 5) and figure-of-eight (Figure 6) trajectories, for clockwise and anticlockwise rotations of the variable stiffness mechanism.

The position variation Δx is fundamental in characterising the displacements of the two racks and, consequently, of the two pairs of springs, allowing the stiffness of the entire system to be adjusted.

In line with what has been reported in the literature [36, 37], the designed VSJ-VSA module is made up of two pairs of antagonistic springs, R_1 and R_2, mounted on either side of the racks. The elongation and compression of these springs allow the stiffness of the system to be adjusted.

As shown in Figure 7, starting from an equilibrium position, when the joint rotates anticlockwise, the spring R_1 stretches, while the spring R_2 compresses, resulting in a change in stiffness that acts as

https://doi.org/10.1017/S0263574725102671 Published online by Cambridge University Press

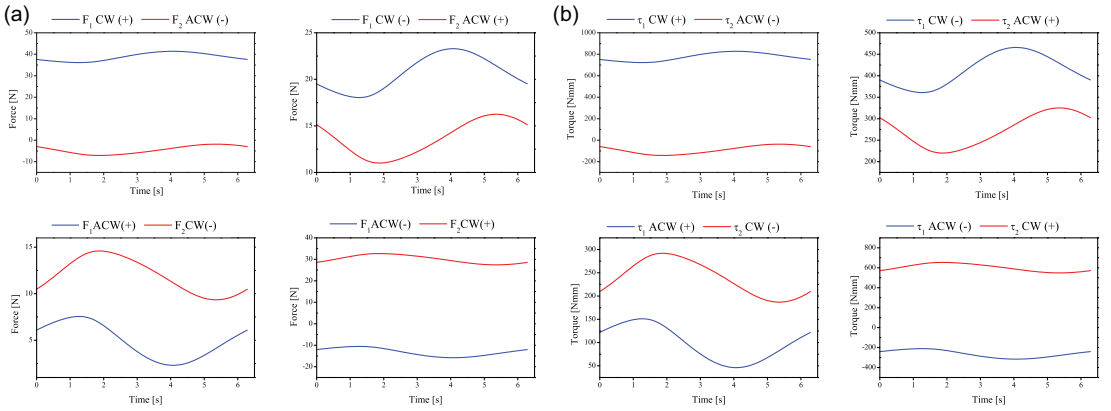


Figure 5. *Results for the circular trajectory: (a) force values; (b) torque values.*

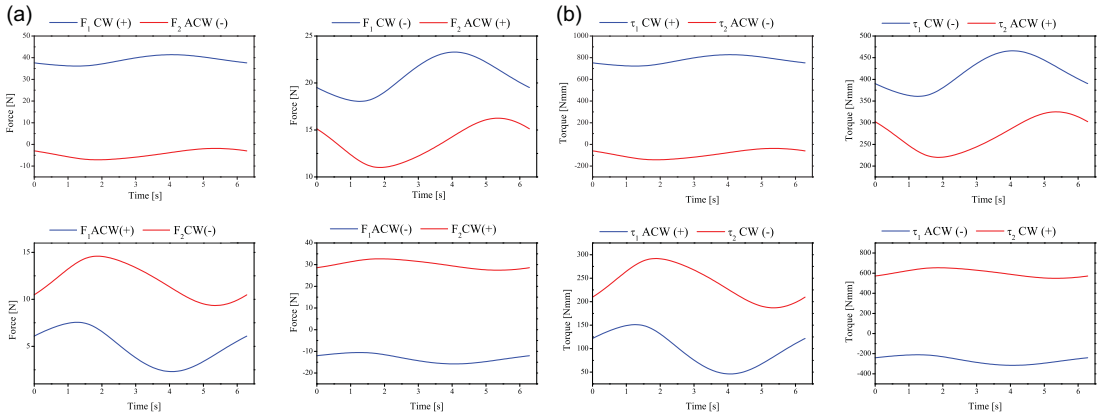


Figure 6. *Results for figure-of-eight trajectory: (a) force values; (b) torque values.*

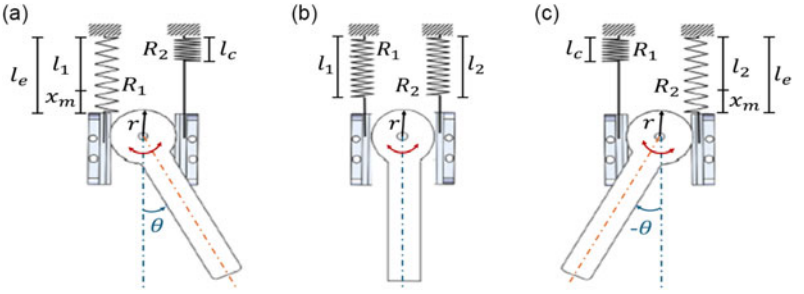


Figure 7. *Diagram of the designed VSJ-VSA module: (a) anticlockwise rotation; (b) equilibrium position; (c) clockwise rotation.*

resistance to the rotation of the connection. In contrast, when the joint rotates clockwise, the spring R_2 stretches, while the spring R_1 compresses.

This concept takes advantage of the properties of the springs to establish the relationship between joint stiffness and resistance force at the end of the connection, according to the rotation angle. As the springs extend or compress depending on the direction of rotation, this directly affects the generated resistance force. In the equilibrium position, the springs are at their natural length and will either stretch or compress with changes in the rotation angle. A larger angle increases the resistance force, creating progressively greater force at the end of the connection.

https://doi.org/10.1017/S0263574725102671 Published online by Cambridge University Press

To maintain constant force at all angles, the length of the springs must be adjusted, ensuring a consistent resistance force during rehabilitation exercises. The variation Δx is expressed as:

$$\Delta x = l_S \pm d_L \mp d_U \tag{13}$$

Specifically, l_S corresponds to the natural length of the springs, while d_U and d_L represent the variations in the positions of the upper and lower racks. The value of d_U is determined by the product of the gear ratio i, which occurs between the pinion and the gear wheel, and the rotation of the pinion. For d_L, it is determined by the ratio between the radius of the gear wheel and the angle of rotation of the encoder.

$$d_U = i \cdot \pi D_P = \frac{Z_P}{Z_G} \cdot \pi m Z_P \tag{14}$$

$$d_L = r_G \cdot \theta_G = r_G \cdot \theta_E \tag{15}$$

where:

- D_P and r_G are, respectively, the number of teeth on the pinion and the gear wheel;
- Z_P and Z_G are, respectively, the diameter of the gear wheel and the radius of the pinion;
- θ_G and θ_E are, respectively, the rotation angle of the gear wheel and the rotation angle of the encoder.

Unlike control-based stiffness modulation, e.g. via PID (Proportional Integral Derivative) tuning, the proposed mechanism achieves intrinsic hardware-level stiffness adjustment. This physical modulation ensures a safe and predictable force response even during failure of the control system or external perturbations, thus offering a redundant and robust solution essential for rehabilitation scenarios involving patients with reduced muscular control.

3. ReHArm prototype: architecture and mechanical design

The ReHArm prototype is designed to ensure flexibility, adaptability, and ease of use in the rehabilitation process. It offers a high level of customisation, with constant resistance, precise control, and the ability to adapt to the specific needs of each user and the different phases of rehabilitation. Accurate adjustment of resistance and stiffness is essential for upper limb recovery, helping to improve muscle strength, joint stability, and neuromuscular coordination. Its compact size (822 × 170 × 236 mm) and low weight (2.5 kg) facilitate transport and installation, making it suitable for both clinical and home settings.

3.1. Configuration and device structure

The variable stiffness device, designed for physical and motor rehabilitation of the upper limb, incorporates multiple hardware components to provide a versatile and effective solution. The structure, shown in Figure 8, consists of six main modules: a mechatronic system, two table clamps for stable installation, a 5-bar mechanism, a pantograph, an optical module, and an ergonomic handgrip.

The mechatronic system comprises two identical modules featuring variable stiffness coupling and actuation (VSJ-VSA) arranged in a mirror image configuration, shown in Figure 9. These modules adjust the stiffness of two pairs of springs in an agonist–antagonist configuration and are powered by two motors with a nominal torque of approximately 2.4 Nm, operating at 12.0 V and 4.4 A. The motors were chosen for their good compromise between torque, compact size, and ease of integration. Although the nominal torque is low, the gearbox provides a mechanical advantage that allows the system to meet the upper limb resistance needs for moderate to severe rehabilitation.

Each module includes custom components, such as top and bottom plates with linear guides for precise movement of the rack-connected carriages. Additionally, the system is enclosed in protective

https://doi.org/10.1017/S0263574725102671 Published online by Cambridge University Press



Figure 8. *CAD model of the ReHarm prototype, illustrating the overall structure and main modules.*

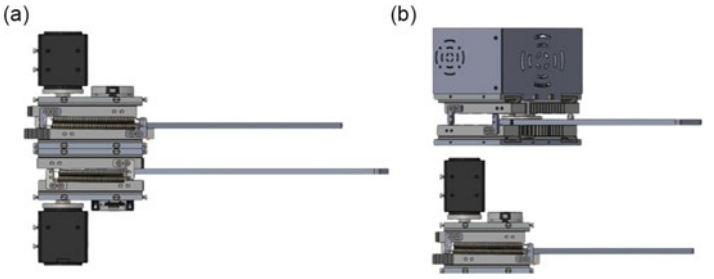


Figure 9. *CAD model of variable stiffness mechatronic system: (a) double VSJ-VSA module without cover; (b) single module with and without cover.*

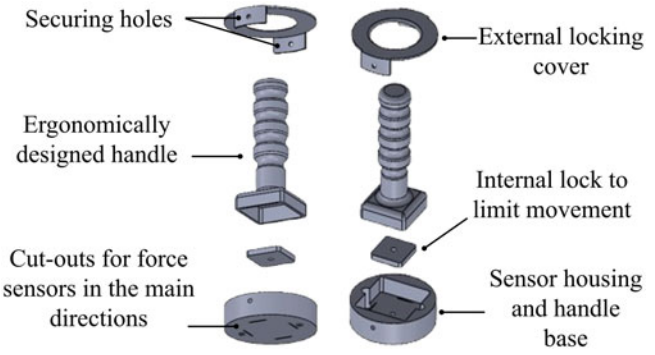


Figure 10. *Device handle: CAD model of the overall structure and components.*

covers that improve safety, assembly, and heat dissipation through ventilation slots. Operation is via a shaft and pinion that drive a gear train to move the racks, thereby adjusting the extension and compression of the springs. Interaction with the 5-bar mechanism translates this movement into a functional action, allowing for precise and customisable stiffness adjustment.

The 5-bar mechanism, connected to the mechatronic system, transmits the stiffness adjustments to the user's movements, while the pantograph extends the ROM, offering greater flexibility. An optical sensor, protected by a cover and harmonised in design, is integrated at the end of the pantograph, which accurately detects user movements, facilitating real-time monitoring and feedback.

Finally, the handle (Figure 10) is ergonomically designed and composed of four distinct modules. Its key feature is the integration of four internal force sensors, which enable accurate measurement and stabilisation of applied forces throughout the rehabilitation process. This ensures a highly personalised treatment and precise control over the interaction between the user and the device.

https://doi.org/10.1017/S0263574725102671 Published online by Cambridge University Press

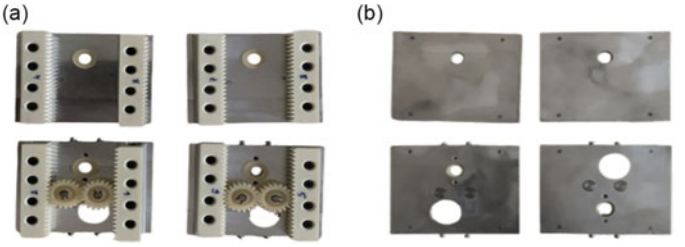


Figure 11. *Prototyping and assembly of plates and components: (a) front view; (b) rear view.*

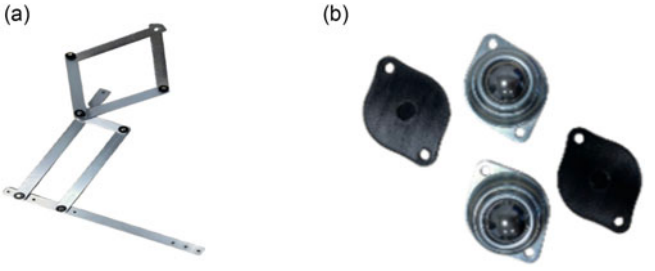


Figure 12. *Prototyping and component assembly: (a) module consisting of the 5-bar mechanism and the pantograph; (b) detail of the omnidirectional wheels and spacers.*

3.2. Modular design and material selection

The device design combines precision mechanical engineering and design optimisation, using 3D modelling to accurately define geometries and dimensions, avoid interference in assembly, ensure modularity, and optimise the choice of materials and technologies to balance strength, lightness, and durability.

The main plates (Figure 11), the fundamental structural element of the VSJ-VSA module, are made of aluminium alloy, both for its excellent mechanical properties and a professional design that enhances the perception of quality. The machining was carried out with precision using CNC machines, which ensured adherence to extremely tight dimensional tolerances and accurate, error-free installation of all mechanical components integrated in the system.

Structural elements such as guides and drive shafts are made of carbon steel C35 for its optimal balance of machinability, strength, and hardness. The shafts are also customised with specific geometries to ensure secure attachment of the gear wheels and prevent slippage or misalignment during operation.

The module's variable stiffness system, as described in the previous section, is based on an ingenious optimised gear train with several components. Specifically, a pinion and two driven wheels allow the translational movement of the upper racks, while, in parallel, an additional gear wheel, directly connected to the 5-bar mechanism, is responsible for the movement of the lower racks. The gear wheels and racks, made of the self-lubricating technopolymer Iglidur, ensure smooth and reliable operation, reducing friction by releasing microscopic amounts of solid lubricant during use, eliminating the need for regular maintenance, and improving the system's durability and efficiency.

In the module with a 5-bar mechanism and pantograph (Figure 12), both made of aluminium, spacers have been placed to ensure correct alignment and levelling with the working surface, while two omnidirectional wheels on the end link reduce friction and improve the smoothness of movement.

3.3. Prototyping technologies and functional components

To complete the variable rigidity system, 3D printing was integrated to reduce prototyping time and costs, allowing essential components and functional supports to be produced in PLA (Polylactic Acid, a biodegradable thermoplastic polymer).

https://doi.org/10.1017/S0263574725102671 Published online by Cambridge University Press

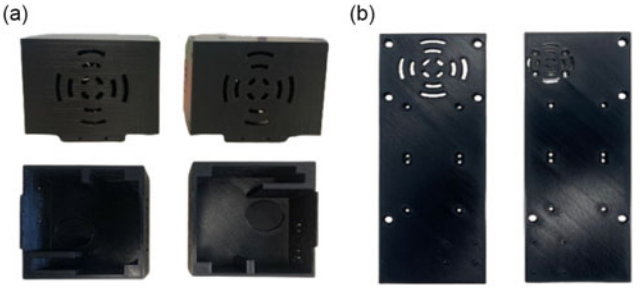


Figure 13. *Prototyping components: (a) top and bottom covers; (b) side covers.*

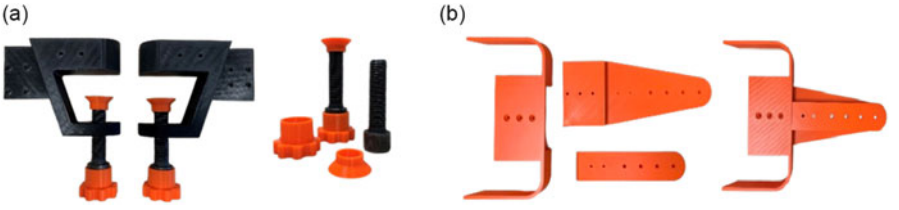


Figure 14. *Prototyping components: (a) clamps with screw and protective covers; (b) components of the triangular structure with related assembly.*



Figure 15. *Prototyping components: (a) optical sensor housing cover, locking cover, and associated circuitry; (b) handgrip hardware components and final assembly.*

The protective covers (Figure 13) not only play a crucial role in external agent protection but are also designed to actively contribute to heat dissipation, thanks to a series of strategically placed slots in the vicinity of the engine to aid heat dissipation.

The device mounting system (Figure 14) has been designed with an optimised structure to ensure functional integration and allow installation on various work surfaces. The configuration includes two clamps paired with a triangular element, which improves the overall stability of the system, optimises the mechanical interface with the pantograph, and ensures safer, more efficient, and more reliable operation.

In addition, advanced ergonomic and functional solutions, such as the optical sensor housing and handgrip, were developed to meet the specific requirements of clinical and rehabilitation applications.

The optical sensor housing (Figure 15a) is a modular system consisting of two separate components, connected to the last link of the pantograph. This configuration guarantees a direct and highly precise transmission of the patient's movements to the customised user interface, without any reduction in sensitivity or precision. The decision to position the modules in this strategic configuration is aimed at optimising the patient's natural movement and minimising fatigue during use. The housing allows for intuitive and direct control, enhancing the user experience and facilitating use by patients with motor disabilities or complex rehabilitation needs.

https://doi.org/10.1017/S0263574725102671 Published online by Cambridge University Press

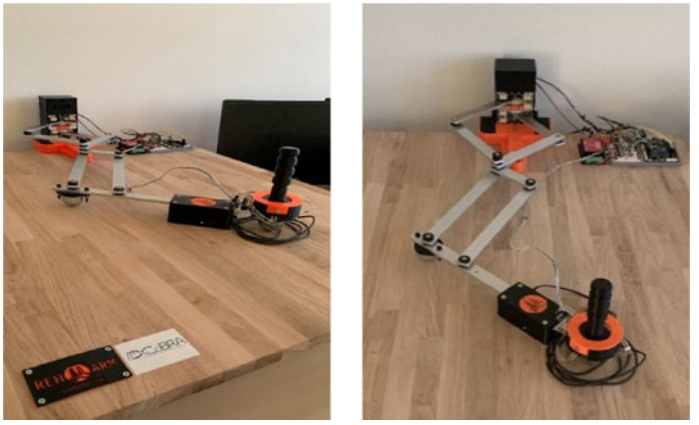


Figure 16. *Configuration and final assembly of the ReHArm prototype device.*

The handgrip (Figure 15b) represents an innovative functional design, structured with a modular approach comprising four main components. Developed with ergonomic and functional requirements in mind, it ensures maximum user comfort without sacrificing control or precision. The base incorporates force sensors that detect the pressure applied by the user, enabling precise movement replication within the interface and dynamic adjustment of stiffness levels during operation. A mechanical lock within the handgrip limits unintended movements, ensuring that the system responds only to intentional actions and reducing operational errors. Designed for ergonomics, the handle adapts to the shape of the hand, minimising fatigue during extended use. In addition, a locking cover enhances stability and safety and strengthens the connection to the pantograph.

This modular configuration allowed the development of the device shown in Figure 16, which features a compact, lightweight, and highly manageable design, offering significant improvements over existing market solutions. The system, including the two VSJ-VSA modules, measures 200 × 72 mm, while the complete prototype, with all integrated modules, has a length of 822 mm, a width of 170 mm, and a height of 236 mm. Optimised material selection and design reduce the total weight to approximately 2.5 kg, ensuring portability and ease of use. Its advanced ergonomics and functional performance make it highly versatile and suitable for various clinical and rehabilitation applications. The design ensures a precise and efficient response to user needs, combining reliability, practicality, and usability.

4. A.R.M.S: user interface design and implementation

The A.R.M.S. user interface, developed for the ReHArm prototype, supports upper limb rehabilitation by improving effectiveness, accessibility, and user involvement. Intuitive and customisable, it simplifies interaction with the device and promotes gradual, motivating progress. The interface is divided into five main scenes, each with a specific function, making navigation easier and guiding users through rehabilitation by integrating key elements such as the database, stages, and gameplay for a more engaging experience.

The database allows doctors and patients to create and manage accounts, storing personal data to enable personalised and engaging treatment. The stages are divided into three progressive levels, guiding users from simple movements to more complex exercises that increase range and frequency.

The gameplay features control of a spherical robot via the device's handgrip. Users collect coins to unlock new levels, with visual and auditory feedback enhancing engagement, making rehabilitation more intuitive, motivating, and rewarding.

4.1. Layout, design, and interface elements

Upon starting the interface, the "Main Menu" (Figure 17a) is displayed, allowing users to access the other scenes. Navigation is intuitive: Users can select options using the keyboard or close the application.

https://doi.org/10.1017/S0263574725102671 Published online by Cambridge University Press



Figure 17. *A.R.M.S. interface: (a) Main Menu; (b) New User ID Menu; (c) Login Menu.*



Figure 18. *A.R.M.S. interface: (a) Options Menu; (b) Audio settings detail; (c) Video settings detail.*

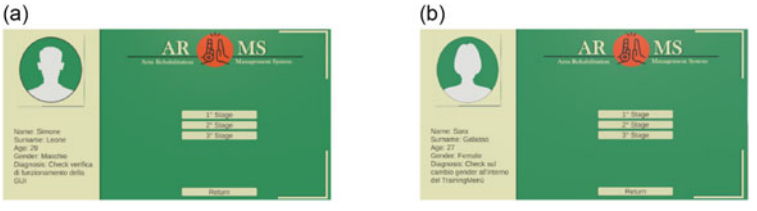


Figure 19. *A.R.M.S. interface: (a) Training Menu with male iconography; (b) Training Menu with female iconography.*

From the Main Menu, users can access the "New User ID Menu" (Figure 17b), where the therapist or user can create profiles, saved in the database. The scene contains seven input fields: four for personal information, two for a username and password, and one for diagnosis.

The users then go to the "Login Menu" (Figure 17c) by clicking "Next". Here, they log in using credentials pre-registered or created earlier. After logging in, they can click "Next" to access the "Training Menu" or return to the Main Menu.

The "Options Menu" (Figure 18a) is dedicated to customising the system settings. It includes three main buttons: Audio, which allows volume adjustment via a slider (Figure 18b); Video, which lets users choose the most suitable resolution (Figure 18c); and Return, which navigates back to the Main Menu.

The "Training Menu" (Figure 19) is the core of the interface, providing access to the rehabilitation stages. On the left, it displays a gender-specific icon, male (Figure 19a) or female (Figure 19b), and the personal data of the registered user. On the right, it includes the Return button to navigate back to the main menu and three buttons that grant access to the respective stages, described in the next section.

4.2. Architecture of rehabilitation stages

The rehabilitation stages are the core of the A.R.M.S. interface, designed to assist users through rehabilitation by providing a continuous, visual, dynamic, and motivating feedback loop.

Each level guides a spherical robot along predefined paths to collect coins, essential for progressing to the next stage. Users access three main stages, each offering a structured rehabilitation path with levels that target specific movements and goals. These stages provide a progressively increasing challenge, balancing entertainment and rehabilitation effectiveness. Specifically:

https://doi.org/10.1017/S0263574725102671 Published online by Cambridge University Press

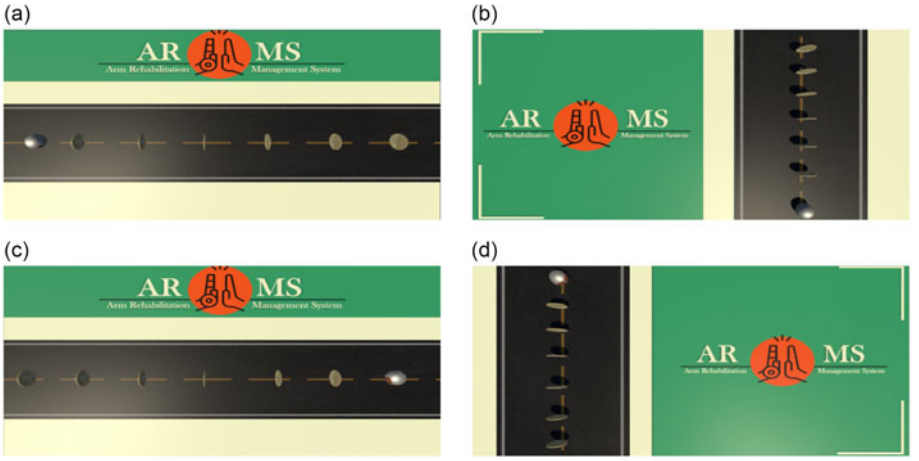


Figure 20. *Levels of the 1st stage and their basic movements: (a) from left to right; (b) from bottom to top; (c) from right to left; (d) from top to bottom.*

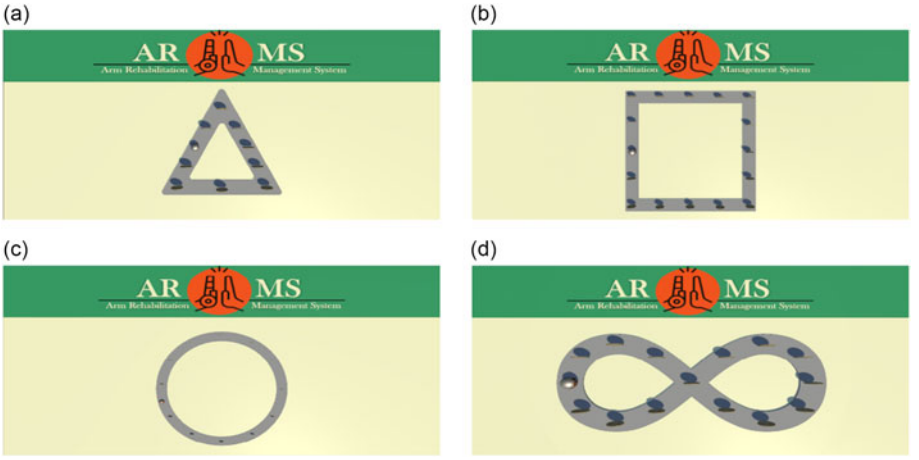


Figure 21. *Levels of the 2nd stage and their trajectories: (a) triangular trajectory; (b) quadratic trajectory; (c) circular trajectory; (d) infinity symbol trajectory or inverted figure eight.*

1st Stage – This stage is designed to help users regain strength and control of their upper limbs through a series of basic movements, minimising stress and fatigue. It consists of four levels, each focused on a different movement (Figure 20), with the completion of one level unlocking the next.

2nd Stage – This stage focuses on combining basic movements to create more complex patterns. This stage also consists of four levels that offer four distinct trajectories reminiscent of geometric elements such as triangle, square, circle, and infinity, shown in Figure 21. This stage aims to improve eye–hand and muscle coordination and movement control, refining the patient's motor skills.

3rd Stage – This final stage offers an advanced rehabilitation mode, which aims to improve the total dexterity and precision of movements. Once the stage is selected, a panel opens that allows users to customise their rehabilitation path by manually entering the dimensions (width and length) of the maze, which will be automatically generated once the "Next" button is pressed, as shown in Figure 22. The user is then asked to experience a new level of challenge, expanding the range of possible movements and consolidating the motor skills learned in the previous stages.

https://doi.org/10.1017/S0263574725102671 Published online by Cambridge University Press

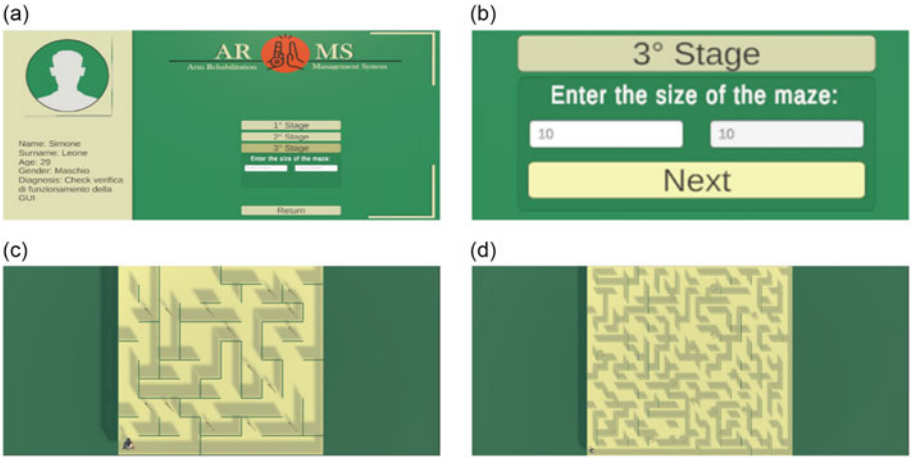


Figure 22. *Level of the 3rd stage: (a) button selection; (b) size insertion detail; (c) 10 × 10 random maze generation; (d) 20 × 20 random maze generation.*

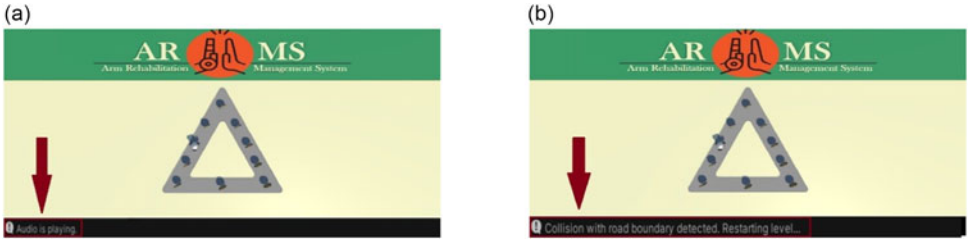


Figure 23. *Detail of the feedback: (a) coin collection; (b) collision.*

Although stages are primarily structured around gameplay complexity, they have been informed by standard clinical assessment tools [38]. The first stage aligns with patients in Brunnstrom stages I–III or FMA (Fugl-Meyer Assessment) upper limb scores below 20, suitable for MRC (Medical Research Council) grades 2–3 (active movement with gravity eliminated). The second stage targets patients in stages III–IV (FMA scores between 20 and 40, MRC grades 3–4), while the third stage is best suited for patients with almost complete voluntary movement (Brunnstrom V–VI, FMA ≥ 40, MRC grade ≥ 4).

Upon completing each stage, the user sees a completion screen with a success sound, which encourages them to continue. Selecting "Next" takes them back to the "Training Menu", where they can repeat the stage, move on to the next one, or close the application. The stages follow a gradual progression designed to motivate the user to improve their motor skills in a safe and effective way.

4.3. Interactive dynamics and gameplay

The core components of the A.R.M.S. interface that ensure a therapeutic and engaging rehabilitation experience are its interactive dynamics and gameplay mechanics. The interactive dynamics are designed to encourage user engagement through linear navigation and increasing difficulty levels with immediate feedback. They start with simple tasks, which gradually become more complex, allowing for progressive improvement of motor skills without causing frustration to users.

The interface provides real-time feedback to enhance the experience and encourage the user to focus and practice during rehabilitation. If a correct movement is made, such as collecting coins, a specific sound is played (Figure 23a) before the coins disappear. If an error occurs, such as going off the path, negative feedback in the form of vibration is triggered, and the level restarts (Figure 23b).

https://doi.org/10.1017/S0263574725102671 Published online by Cambridge University Press

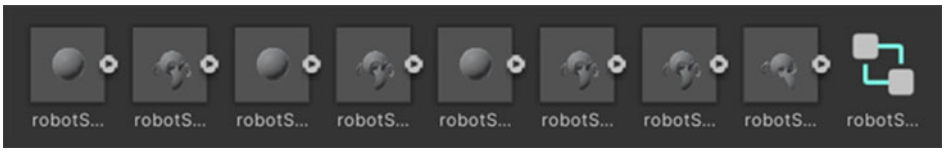


Figure 24. *Animation structure of the robot within the A.R.M.S. interface.*

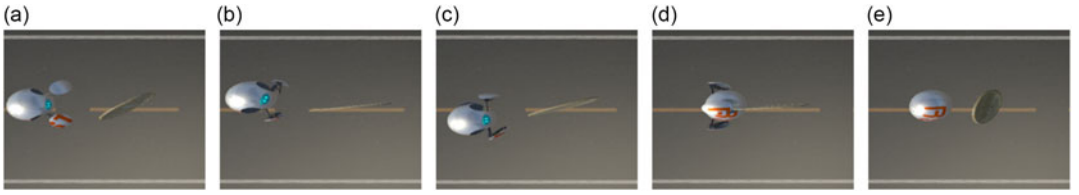


Figure 25. *Photogram of the animation of the robot inside the A.R.M.S. interface.*

The gameplay itself is designed to fully immerse users in the process, ensuring both therapeutic effectiveness and engagement. Users control a spherical robot whose movement is directly linked to the prototype handgrip, establishing an immediate connection between the user's input and the robot's actions. Before starting its journey, the robot grabs the user's attention with an introductory animation, as illustrated in Figure 24.

The animation sequence begins with the robot opening, followed by short preparatory movements before it starts rolling, as shown in the frames in Figure 25. At the end of the animation, the user can control the robot via the handle, guiding it along the path and collecting coins to access the next stages.

The robot's movement is controlled by a series of scripts that govern the interaction between the device and the user, translating the user's movements into real-time actions in the rehabilitation interface. Although similar across the different stages, the scripts have some differences in how they handle inputs. In the first phase, for example, horizontal inputs (X) are used for the first and third levels, while vertical inputs (Y) are used for the other two. In the second and third phases, optical sensor inputs are handled uniformly across all levels, with the addition of specific handling for different types of boundaries (triangular, square, maze walls, etc.) and for coin collection.

When a level is restarted, the system temporarily disables the robot's sensors, resets its position and rotation to the initial state, and reactivates the sensors to allow the user to regain control.

4.4. User management system and database

The user management system in upper limb rehabilitation plays a crucial role in ensuring efficient and secure patient data management. The database, designed to reliably store patient information, is essential for coordinating registration, authentication, and monitoring therapeutic progress.

User profiles are created via the "New User ID" menu, where personal details, a unique ID, password, and diagnosis are entered. This data is stored in JSON format, ensuring flexible access and optimised management while reducing retrieval time. After registration, users log in, and upon authentication, they are directed to the Training Menu, where the three rehabilitation stages are available.

Beyond data management, the database collects key rehabilitation metrics, including exerted force, accuracy of movement, and completion of exercise. This information provides graphical feedback, helping both patients and healthcare professionals assess and refine treatment plans. The system gathers data in real time using force sensors in the handgrip to measure intensity and encoders in the motors to track movement position and speed. Graphical reports illustrate rehabilitation progress: strength and control variations in initial movements (Figure 26a), accuracy and trajectory completion in geometric exercises (Figure 26b), and impact of maze difficulty on task completion (Figure 26c). By visualising these trends, the system ensures a more effective and adaptive rehabilitation process.

https://doi.org/10.1017/S0263574725102671 Published online by Cambridge University Press

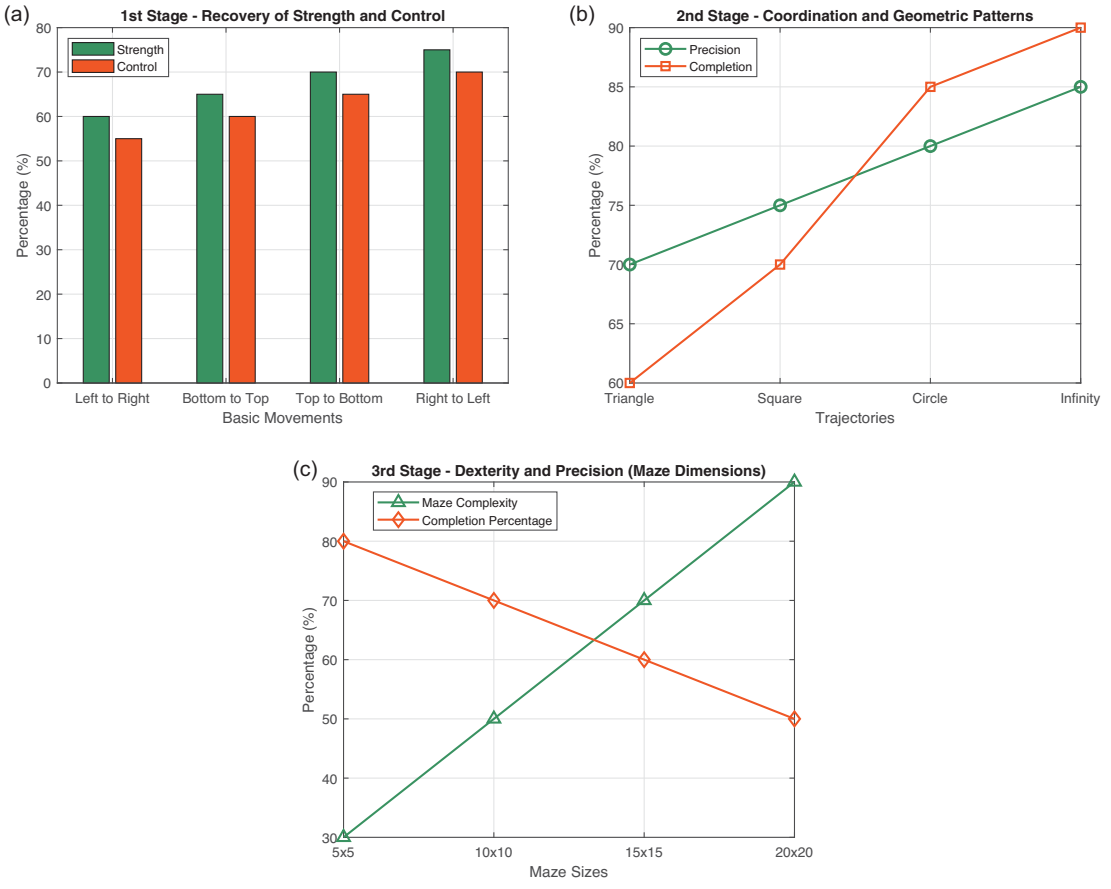


Figure 26. *Rehabilitation progress across different stages: (a) strength and control during basic movements in the 1st stage; (b) accuracy and trajectory completion in the 2nd stage; (c) effect of maze difficulty on task completion in the 3rd stage.*

5. Control architecture

This chapter examines the control architecture and communication between the variable stiffness device and the control interface, based on previous analyses and results. It outlines the architecture of the control system, the selection and calibration of sensors, and the communication between the device and the interface to ensure reliable transmission of data and commands. The Arduino platform was chosen to implement the control code due to its flexibility, ease of use, and efficient device management.

5.1. Hardware system configuration and implementation

To ensure effective monitoring of interaction dynamics and a customised approach in rehabilitation, a force sensing system and advanced control architecture were implemented.

The OpenCR board was selected for its advanced features, including an integrated processor with peripherals, an intuitive development environment, and a wide range of connections. In addition, the robust real-time operating capabilities and embedded communication protocols of the board ensure stable performance even in complex rehabilitation scenarios involving dynamic external forces. This configuration connected the entire hardware system, consisting of servomotors, encoders, and force sensors. This was essential to efficiently coordinate signal acquisition, motor control, and encoder management.

https://doi.org/10.1017/S0263574725102671 Published online by Cambridge University Press

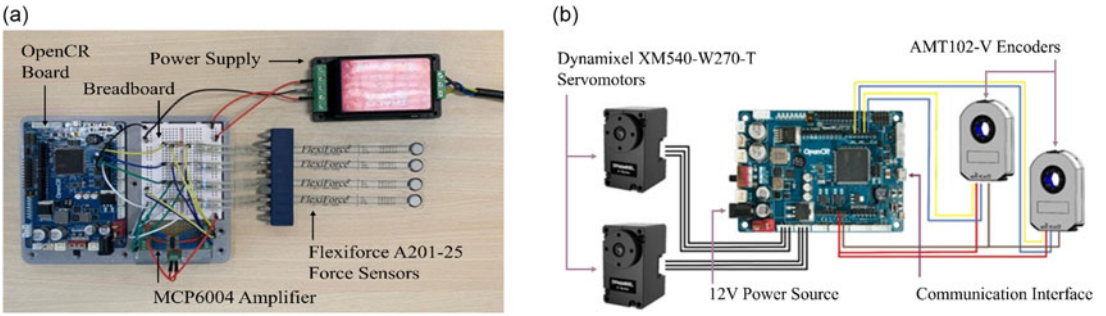


Figure 27. *Hardware setup: (a) signal acquisition circuit for force sensors; (b) servomotor and encoder connection diagram.*

Four FlexiForce A20-251 sensors were used for force detection, with a maximum load of 110 *N*, a choice guided by their high sensitivity, precision, and reliability. In addition, their electronic compatibility and installation flexibility allowed optimal integration in the device's handle to monitor interaction dynamics. The strategically placed sensors detect forces in the horizontal and vertical directions, as well as combined effects, ensuring accurate measurement.

To ensure optimal acquisition of signals from the sensors, an electronic circuit designed in accordance with the manufacturer's recommendations was implemented. At the heart of this circuit is an operational MCP6004 amplifier, configured to optimise the signal-to-noise ratio and provide a stable response even in the presence of pressure variations. The sensors have been integrated into the circuit using an operational amplifier with a 47 pF capacitor and a 100 kΩ feedback resistor, elements that stabilise the amplified signal and guarantee linearity. To ensure correct operation, a dedicated power supply system was implemented with symmetric + 5V and −5V voltages. This configuration, visible in Figure 27a, allowed one to obtain a stable signal proportional to the applied load variations.

In addition to the force sensors, the hardware components of the two variable stiffness modules – consisting of two Dynamixel XM540-W270-T servomotors and two AMT102-V encoders – are also connected directly to the OpenCR board. These components are essential for stiffness management and position detection of the device during user interaction. The adopted configuration, visible in Figure 27b, allows synchronous integration of sensor signals with feedback provided by the encoders and the control of the servomotors, thus ensuring precise and coordinated operation of the prototype.

By monitoring the position detected by the encoders in real time and adjusting the movements of the servomotors via the OpenCR Board in relation to the sensor data, it is possible to achieve efficiency, stability, and precision in both data acquisition and system response. The control system incorporates real-time filtering algorithms and fail-safe routines executed on the OpenCR board to quickly detect and compensate for sudden external disturbances or sensor anomalies, thus maintaining operational stability under unpredictable conditions. This approach optimises the performance of the prototype during the rehabilitation process by adapting the behaviour of the device to the specific needs of the user, thus improving the experience and effectiveness of the system.

5.2. Calibration and configuration of control system components

To ensure precision in data collection, efficient operations management, and effective control logic, a structured process of calibration and configuration of the main control system components was conducted. In particular, force sensor calibration and motor configuration were performed following rigorous iterative procedures, supported by dedicated tools. These steps ensure that the control logic operates with maximum effectiveness and reliability, optimising overall system performance.

Before calibration, the force sensor underwent a "running-in" phase, with an iterative load at 110% of the maximum expected value, maintained for 3 s. This procedure stabilised the characteristics of the sensor, ensuring a consistent response. The calibration was then performed by gradually applying sample

https://doi.org/10.1017/S0263574725102671 Published online by Cambridge University Press

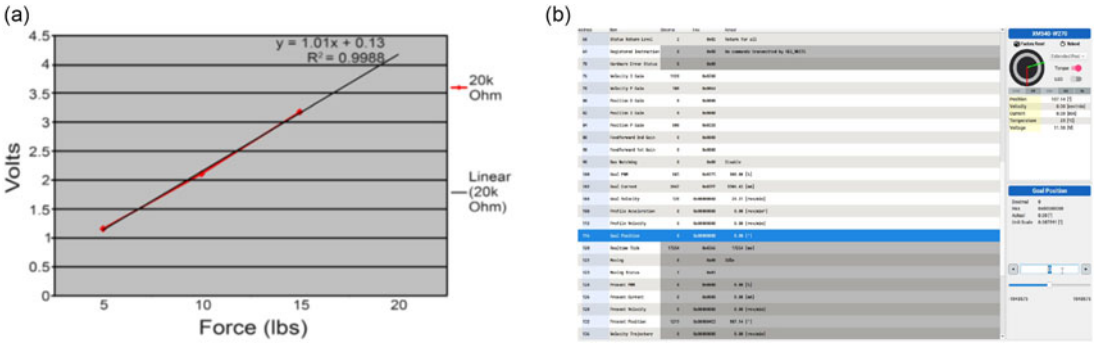


Figure 28. *Calibration and configuration: (a) tension-force graph with trend line; (b) configuration of system motor parameters.*

weights and recording the corresponding output. The data collected were processed using a tension-force graphical representation, which allowed interpolation of the trend line (Figure 28a) and derivation of the characteristic equation. This equation translated the sensor output into an accurate estimate of forces on unknown loads during subsequent experiments.

In parallel, a detailed configuration of the motors in the system was carried out (Figure 28b), defining communication parameters such as the transmission protocol and the baud rate, calibrating position limit, and configuring specific operating modes. These steps ensured a stable interface between the motors and the control system. Additionally, a thorough check of the motors' firmware was carried out and, where necessary, updated to ensure compatibility with the control infrastructure under development. This operation optimised performance, minimising potential motion management issues.

The calibration and configuration process integrated sensors and actuators into the control system, forming a solid foundation for control logic development. These preliminary activities are crucial to ensuring accurate, reliable operation and meeting performance standards.

5.3. Design and implementation of system control logic

The implementation of the control logic required extensive configuration and programming to ensure system efficiency and automation. Based on the analyses conducted, following the preliminary phases, individual component codes were developed, validated, and integrated into a unified control programme.

In the initial phase, fundamental constants and variables were defined to manage servomotor control and force sensor data acquisition. The dedicated pins for encoders and sensors were carefully configured, enabling serial communication for seamless integration of the system. The servomotors were then initialised in an extended mode, allowing precise movement control to optimise functionality.

Subsequently, the force sensor calibration was performed through a series of acquisitions to identify and compensate for systematic signal offsets. This step was crucial in ensuring measurement accuracy while minimising errors caused by operational variations or sensor imperfections. After initialisation and calibration, the system transitioned to the main operational phase, managed within a continuous loop. During this phase, force sensors, motor rotation angles, and encoder values of the 5-bar mechanism were acquired in real time, enabling synchronised monitoring of the system's kinematics and providing a clear overview of its state. Using the mathematical models developed, the system dynamically adjusts the mechanical stiffness of each module by processing force and position data in real time. Specifically, the data from the force sensors and encoders are continuously analysed to precisely regulate the torque applied by the motors, which in turn allows real-time control of the extension and compression of the antagonistic springs. Through this mechanism, the collaborative control between the VSJ and the VSA ensures that, based on the patient's resistance and movement patterns, the appropriate pair of springs is tensioned or relaxed. This enables adaptive and personalised stiffness regulation throughout the rehabilitation session. In addition, the control logic includes redundancy checks and sensor data

https://doi.org/10.1017/S0263574725102671 Published online by Cambridge University Press

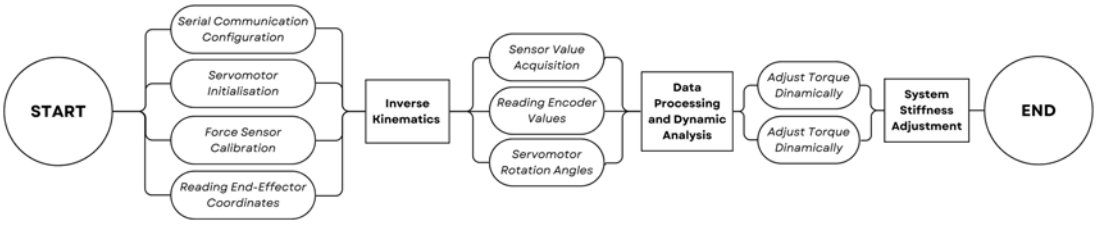


Figure 29. *Flowchart of the implemented control logic.*

validation mechanisms to identify sensor failures or signal inconsistencies. Upon detecting a fault, the system triggers predefined fault-tolerant responses, such as switching to backup sensor inputs or safely halting motor commands, thus enhancing the reliability and safety of the rehabilitation device.

The proposed control logic ensured adaptive resistance modulation based on the detected interaction parameters, optimising the mechanical response. This approach allowed real-time adjustments of mechanical equilibrium, enhancing the system stability, responsiveness, and precision. Consequently, the control system maintained the desired resistance levels, improving both performance and reliability.

For a detailed representation of the approach and system functionality implemented, the flow chart in Figure 29 illustrates the interactions among the main functions and processes of the control algorithm.

5.4. Communication protocol between device and interface

The communication between the ReHArm prototype and the A.R.M.S. interface is designed to ensure precision and reactivity during rehabilitation, thanks to a hardware and software system that translates the user's movements into virtual actions, improving engagement and effectiveness.

The OpenCR board processes signals from sensors, actuators, encoders, and the optical sensor located between the handle and the last segment of the pantograph, which detects the user's movements, converts them into two-dimensional coordinates, and sends them to the interface in real time via a high-speed serial protocol. The interface uses these data to control the virtual spherical robot, the central element of the rehabilitation exercises, following predefined or user-created trajectories and interacting with virtual objects such as coins or obstacles. A mapping algorithm transforms the coordinates into kinematic inputs, synchronising physical movement with visual feedback. An asynchronous control loop constantly monitors sensor data and updates the robot's position in real time. Visual and acoustic feedback makes the experience more immersive and promotes motor learning.

This integrated architecture allows for accurate and natural translation of movements into the virtual context, improving the effectiveness of rehabilitation. The integration of advanced hardware and optimised software makes ReHArm and A.R.M.S. innovative, interactive, and effective solutions in the field of robotic rehabilitation.

6. System testing and evaluation

This section describes the objectives, methods, and results of the testing phase, evaluating the effectiveness of the system in rehabilitation and user experience. The tests were carried out at multiple levels with internal collaborators to ensure the reliability, accuracy, and robustness of the developed system. Particular attention was paid to stiffness adjustment, analysing hardware inputs and user interactions to ensure the immediate translation of movements.

6.1. Sensor validation: accuracy, robustness, and interaction testing

Sensors represent a crucial component within the system, providing essential information for the operation of variable stiffness modules and for monitoring the interaction dynamics with the device.

Following their calibration, a series of tests was conducted to evaluate the accuracy and robustness. The tests followed a cascade approach, analysing each sensor individually in sequence. This method

https://doi.org/10.1017/S0263574725102671 Published online by Cambridge University Press

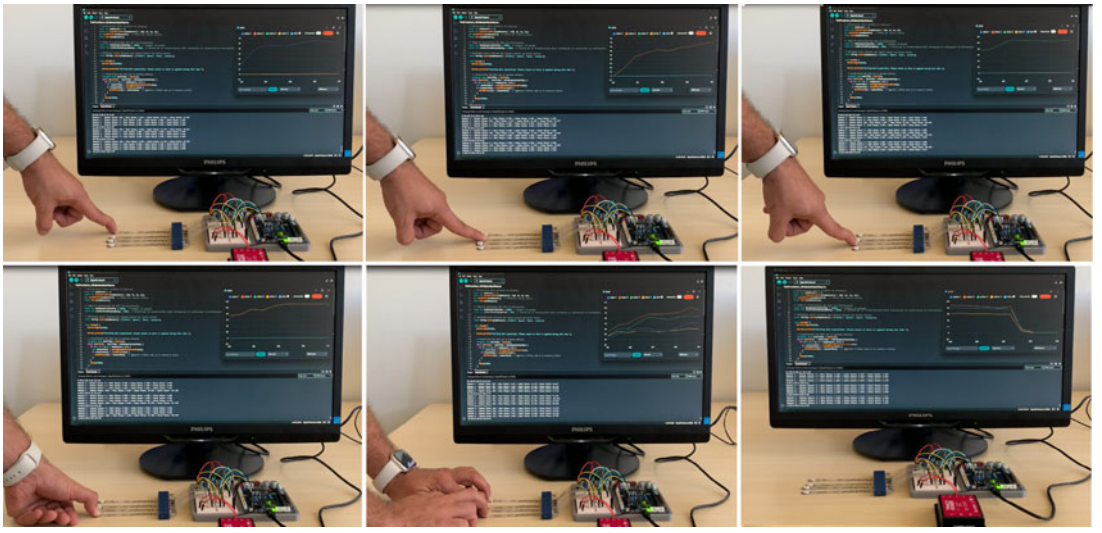


Figure 30. *Sensor testing: evaluation of proper functionality and calibration verification.*

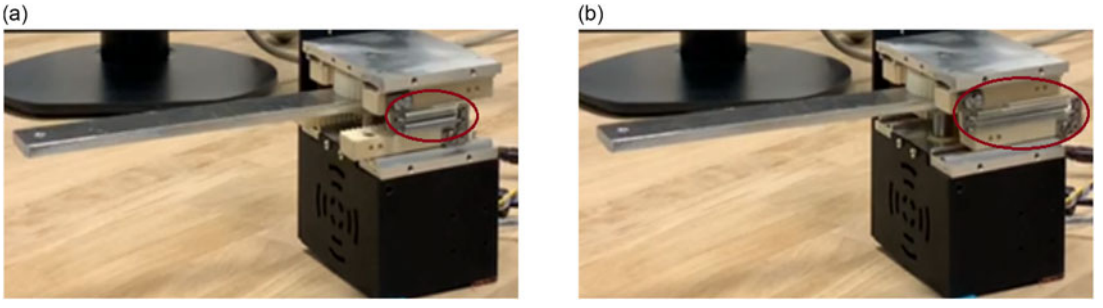


Figure 31. *Tests on individual variable stiffness modules: (a) resting condition of the springs; (b) full pre-tensioning of the springs.*

allowed us to identify any issues and observe sensor performance under different conditions. Subsequently, an integrated test was performed with all sensors active simultaneously to evaluate their consistency and interaction during data acquisition, identifying any conflicts, interference, or anomalies. The results confirmed reliable measurements under all operating conditions, with any discrepancies corrected through software and hardware adjustments, ensuring consistency and accuracy in force monitoring during use.

Figure 30 illustrates the sensor testing, highlighting the evaluation of the correct functionality and the verification of calibration, both individually and as a whole.

6.2. Validation of the variable stiffness module: reliability and performance

The initial test phase evaluated the ability of individual variable stiffness modules to maintain positional stability after removing the external load, verifying the effectiveness of the stiffness control system and identifying any problems with internal energy dissipation. Figure 31 shows the tests on individual modules, with particular reference to the pre-tensioning of the spring pairs, highlighted in red.

Subsequently, phenomena such as the elongation and compression of springs were observed in response to variable rotational movements, with the aim of evaluating their dynamic behaviour under specific adjustment conditions. In particular, three configurations were analysed: clockwise rotation (Figure 32a), equilibrium position (Figure 32b), and anticlockwise rotation (Figure 32c).

https://doi.org/10.1017/S0263574725102671 Published online by Cambridge University Press

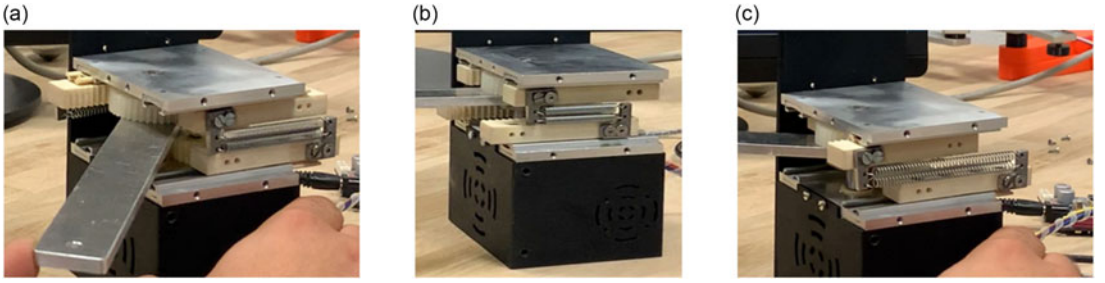


Figure 32. *Tests on the elongation and compression of springs in response to link movement: (a) clockwise rotation; (b) equilibrium position; (c) counter-clockwise rotation.*

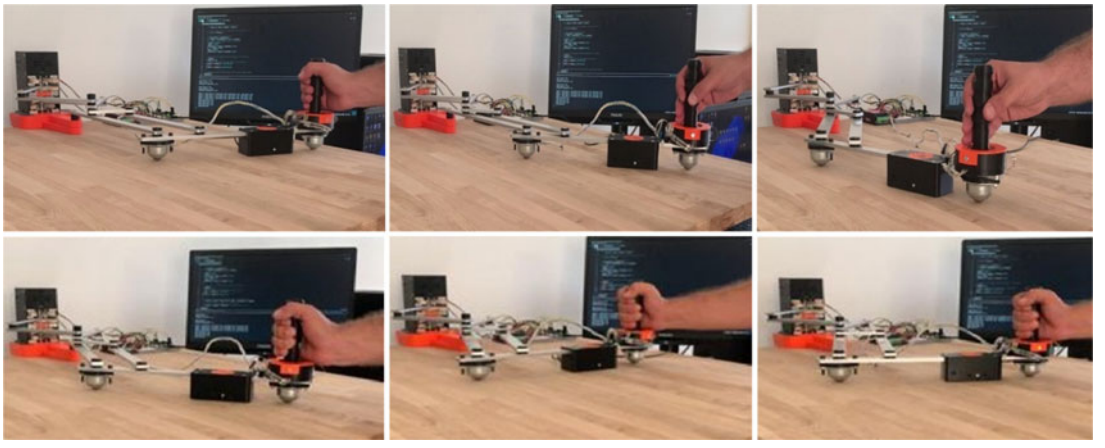


Figure 33. *Tests performed on the entire device.*

These observations proved essential in confirming the stability and predictability of the response of individual components within the expected ROM.

The tests were carried out on the complete device after analysing individual modules to assess their behaviour and interaction between the variable stiffness module and other components under varying stiffness conditions, as shown in Figure 33. Trajectories were evaluated and kinematic tests performed to assess the system's responsiveness to user demands, ensuring stable performance over time.

The behaviour of two pairs of springs in an agonist–antagonist configuration within each device module was analysed. These springs dynamically adapt their stiffness parameters based on device movements and the forces recorded through compression and elongation. Figure 34 shows the variations in compression and elongation of the springs in response to the values recorded during the movement, highlighting their contribution to the load distribution and stability of the device and confirming the effectiveness of the agonist–antagonist configuration in ensuring robustness and functionality.

The test results confirmed the ability of the variable stiffness device to dynamically adapt to the user's needs, providing adequate and comfortable support across a range of operational situations. These preliminary tests confirm the mechanical reliability of the prototype and highlight its potential as a valid support in rehabilitation scenarios, although further clinical validations are required to obtain definitive confirmation of its efficacy.

6.3. Verification and comparison between theoretical and experimental results

To validate the accuracy of the developed kinematic and dynamic model, a thorough experimental verification was conducted through real-world tests replicating the trajectories of interest. Specifically,

https://doi.org/10.1017/S0263574725102671 Published online by Cambridge University Press

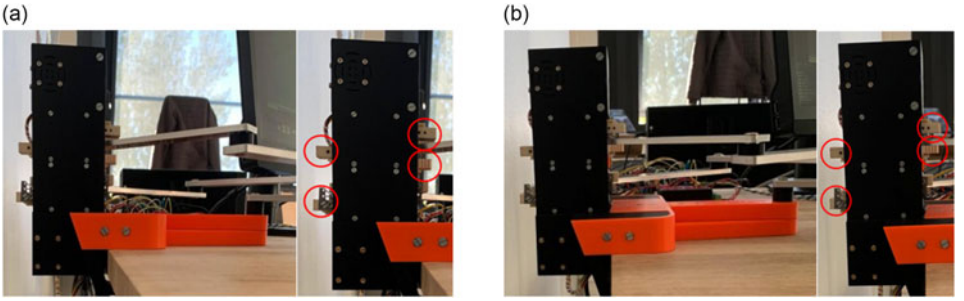


Figure 34. *Tests performed on the entire device: (a) detail of the elongation of the right pair of springs and the compression of the left pair of springs; (b) detail of the elongation of the left pair of springs and the compression of the right pair of springs.*

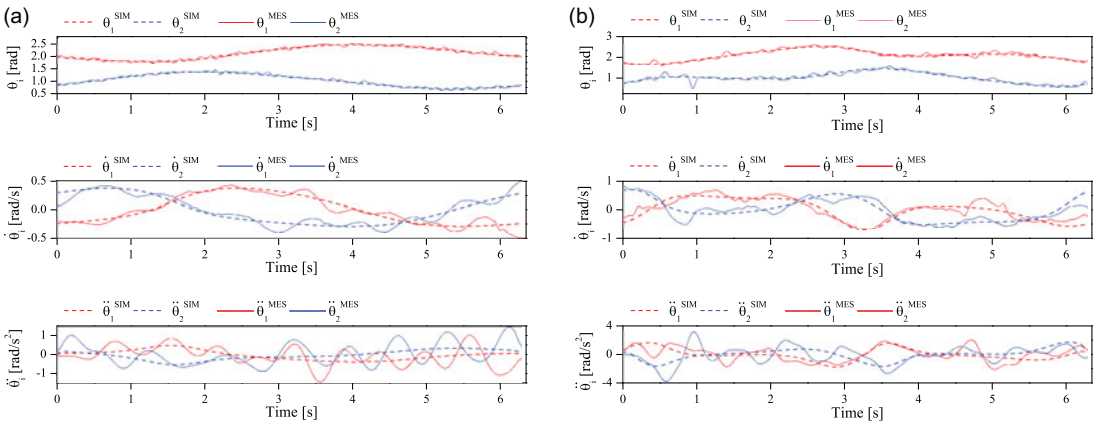


Figure 35. *Comparison of simulated and experimentally measured kinematic parameters of the mechanism: (a) circular trajectory; (b) figure-eight trajectory. The graphs show the time evolution of the position, velocity, and angular acceleration of the main joints (θ_1, θ_2). Simulation results are shown with dashed lines, while experimental data are represented with solid lines.*

experimental measurements were performed along the two investigated paths, the circular and figure-eight trajectories, consistent with what was described in Section 3 above. During these tests, kinematic data, such as position, velocity, and acceleration, as well as dynamic data related to applied forces and torques, were acquired using sensors appropriately positioned on the prototype.

The experimental results of the kinematic variables (position, velocity, and angular acceleration) are illustrated in Figure 35, where the theoretical curves, obtained from the simulation, are compared with those measured for the two trajectories. The analysis shows a good correlation between the simulation and the experimental measurements for both trajectories.

For the circular trajectory (Figure 35a), a substantial overlap between the theoretical and experimental profiles is observed, with minimal deviations mainly attributable to the intrinsic delay of the sensors, the mechanical vibrations present during the motion, and the non-linearities of the control system. The infinite trajectory (Figure 35b) shows similar characteristics of agreement, highlighting the validity of the implemented kinematic model.

Comparison of forces (Figure 36) reveals more marked differences between simulation and experimental measurements. For the circular trajectory (Figure 36a), the measured forces show oscillations and peaks that are not fully captured by the ideal model, suggesting the influence of unmodeled factors such as mechanical friction in the joints, the finite stiffness of the structure, and actuator non-linearities.

https://doi.org/10.1017/S0263574725102671 Published online by Cambridge University Press

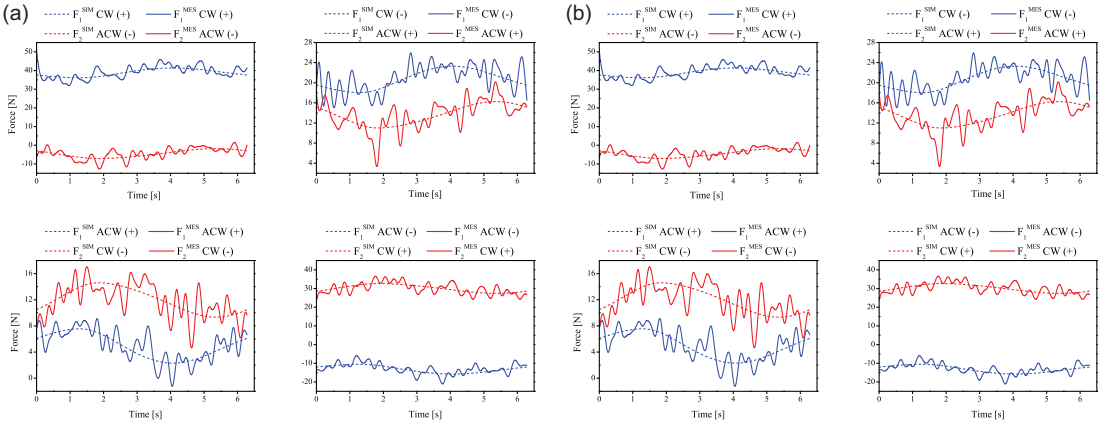


Figure 36. *Comparison of simulated and experimentally measured forces of the mechanism: (a) circular trajectory; (b) figure-eight trajectory. The graphs show the time evolution of the force components: simulation results are shown with dashed lines, while experimental data are represented with solid lines.*

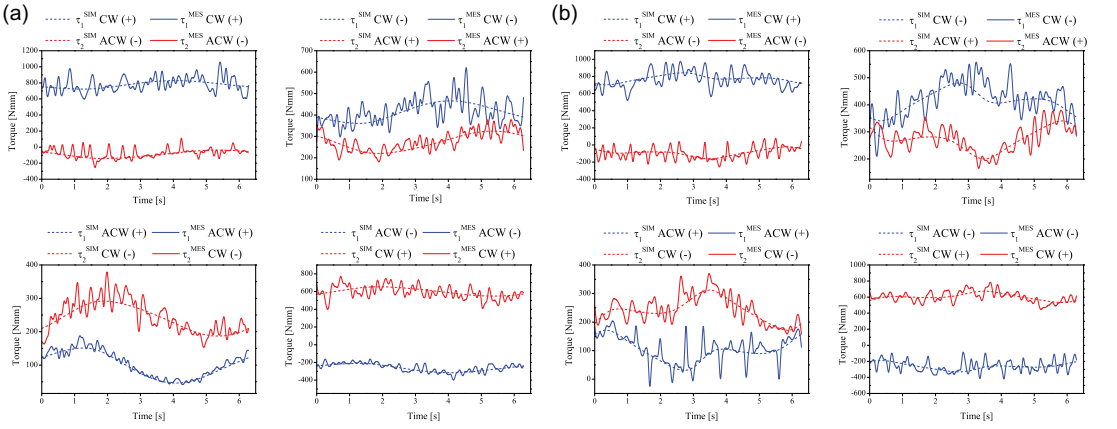


Figure 37. *Comparison of simulated and experimentally measured joint torques of the mechanism: (a) circular trajectory; (b) figure-eight trajectory. The graphs show the time evolution of the torques: simulation results are shown with dashed lines, while experimental data are represented with solid lines.*

Similarly, for the infinite trajectory (Figure 36b), the experimental forces exhibit a higher harmonic content than the simulations, indicating the presence of high-frequency dynamics not considered in the model.

The torque analysis, reported in Figure 37, confirms what was already observed in the force study, highlighting how the experimental measurements exhibit significantly more complex behaviour than the profiles obtained through simulation. The discrepancies between the experimental data and the model are attributable to several unmodeled physical factors that influence the dynamics of the real system. First, the mechanical friction in the gear train and joints introduces non-linear effects not captured by the ideal model. In addition, delays in sensors and control systems cause a time lag between the command and the actual response, affecting the temporal alignment between simulation and experiment. The structural flexibility of the prototype also contributes to the discrepancies, as it introduces modal dynamics that are not accounted for in the rigid-body model. Finally, actuator non-linearities, especially evident during motion reversals, modify the system's dynamic response in ways not predicted by the simulation, increasing the complexity observed in the experimental data.

https://doi.org/10.1017/S0263574725102671 Published online by Cambridge University Press

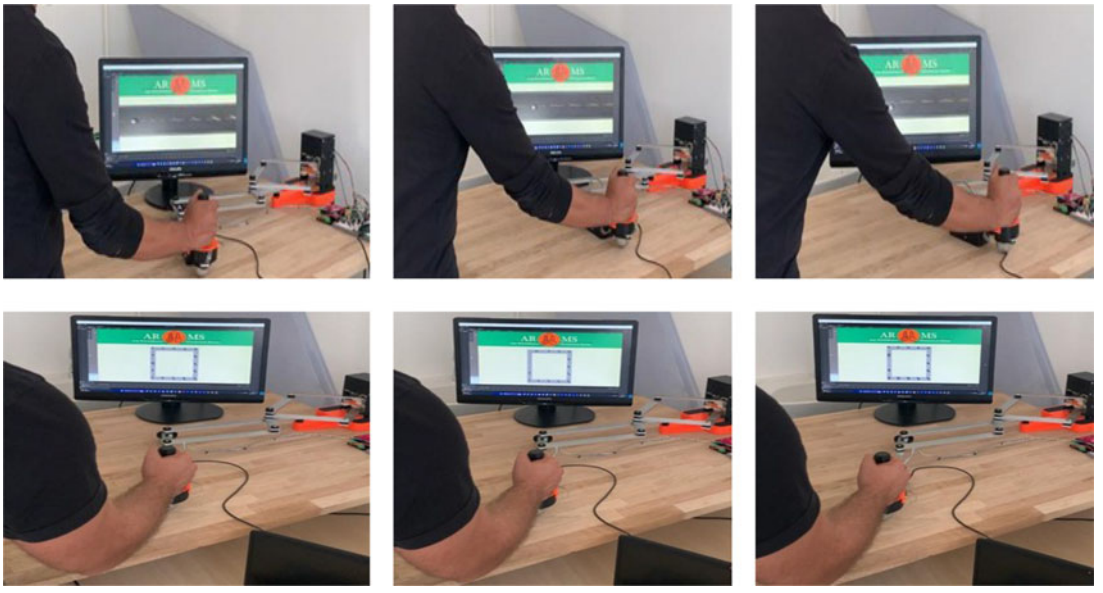


Figure 38. *Usability and responsiveness testing of the A.R.M.S. interface.*

The comparison between experimental data and simulations shows good agreement in both trend and values, confirming the validity of the model in the preliminary design phase and strengthening its reliability for rehabilitation applications. The discrepancies found provide valuable insights for improving the dynamic model, particularly through the inclusion of dissipative effects and a more accurate representation of non-linearities. However, further tests with patients will be necessary to complete its validation in the clinical setting.

6.4. Analysis of testing and user interface optimisations

To ensure proper functionality, debugging tools were initially implemented in various user interface components, enabling real-time monitoring of the system's behaviour and prompt identification of any errors or anomalies during testing. This allowed verifying the correct input of user information into the database and more specific testing, such as reproducing the soundtrack, checking sound and visual feedback, and detecting collisions between the robot and the virtual elements.

Subsequently, an integrated methodological approach was adopted, combining quantitative and qualitative tests to provide a comprehensive evaluation of the performance of the application. The quantitative analysis included the measurement of key indicators, such as task completion time and the success rate in using the main functionalities. In parallel, qualitative testing (Figure 38) was conducted through interviews with a group of internal colleagues who used the system to gather detailed feedback on user experience and usability of the interface.

The results obtained provided a comprehensive view of the performance and critical aspects of the implemented user interface. In particular, the tests conducted with internal users (i.e. colleagues involved in the evaluation process), carried out over multiple iterative cycles, represented a crucial phase in the development process. These testing cycles enabled significant modifications to the system's interactivity on the basis of feedback received.

Specifically, the following aspects were addressed:

- **Input device sensitivity:** The average optical sensor sensitivity was gradually adjusted across different levels in response to user suggestions, ensuring a more natural and responsive experience;

https://doi.org/10.1017/S0263574725102671 Published online by Cambridge University Press

- **Robot movement speed:** Speed parameters were optimised to ensure stable and consistent interaction between the prototype and the user interface, thereby enhancing control and movement fluidity;
- **Introduction of a pad:** A pad was added between the prototype and the working surface to reduce friction during movements, improving the fluidity, precision, and control of the device.

These interventions resulted in a significant improvement in the user experience, addressing critical issues identified during testing and improving the overall performance of the system.

A 25% reduction in the average time required to complete the tasks was observed, along with an increase in the success rate, which improved from 75% to 92% in the execution of rehabilitation stages. While current testing focused on usability metrics such as task completion time and success rate, future clinical trials will include standard rehabilitation effectiveness indicators such as ROM, muscle strength scores, and ADL scales to comprehensively assess therapeutic outcomes. User interviews also highlighted a high level of satisfaction with the application, with positive feedback on its effectiveness as a tool to support the rehabilitation process. Participants consistently described the interface as intuitive, clear, well-structured, and user-friendly.

Despite these promising results, opportunities for improvement were identified, including the integration of a broader range of exercises and the implementation of more advanced customisation options for system settings. These user-driven insights will inform the ongoing development of the device, ensuring that future iterations align more closely with user needs and expectations.

Conclusions

The proposed rehabilitation system, comprising the ReHArm prototype and the A.R.M.S. interface, represents a technologically advanced solution for upper limb rehabilitation, addressing the needs of a healthcare landscape increasingly focused on personalised and effective therapies. The combination of a variable stiffness device and an intuitive, interactive interface provides significant added value in clinical and home-based settings, enhancing accessibility and adherence to rehabilitation.

From an engineering perspective, the modular architecture of ReHArm stands out for integrating advanced mechatronic solutions, including VSJ and VSA, which enable dynamic and precise adjustment of resistance. This adaptability allows therapy to be customised to the specific clinical needs of each patient, improving not only rehabilitation quality but also the overall user experience. The compact and lightweight design ensures ease of handling and installation, making it suitable for diverse environments, supporting treatments ranging from post-traumatic rehabilitation to the management of chronic conditions.

The tests performed in a controlled environment have highlighted the reliability and robustness of the system from a technical point of view, confirming the high precision of the integrated force sensors and the functionality of the solutions adopted for the adaptive regulation of stiffness. Although the results are promising, clinical studies on patients will be needed to evaluate their rehabilitative efficacy and real therapeutic impact. In particular, a detailed analysis of trajectories, the control of 5-bar mechanisms, and the management of kinematic and dynamic parameters have shown that the system maintains stable and consistent performance even in the presence of significant operational variability.

The A.R.M.S. interface, a pivotal element of the rehabilitation system, has proven to be highly innovative in actively engaging patients through a structured rehabilitation pathway composed of progressively challenging stages. The combination of visual and auditory feedback, along with real-time performance monitoring, has facilitated a motivating and immersive interaction, improved treatment adherence, and user awareness of their progress. The structured database management system further allows for the detailed collection and comprehensive analysis of patient progress data, providing healthcare professionals with an invaluable tool for optimising personalised treatment plans.

The results obtained represent a solid foundation for future development of the system. Furthermore, the innovative nature of this work has been protected through the submission of a patent application

https://doi.org/10.1017/S0263574725102671 Published online by Cambridge University Press

(Dossier Number: 102024000006292), demonstrating its originality and scientific and technological significance. The granting of this patent highlights the uniqueness of the proposed solution and its potential impact within the field of robotic rehabilitation.

In conclusion, the ReHArm system and A.R.M.S. interface provide a tangible example of how the integration of robotic engineering, ergonomics, and interactivity can transform the approach to motor rehabilitation. The findings represent a solid foundation for clinical deployment and future iterations to address emerging challenges in assistive robotics and personalised rehabilitation.

Author contributions. S.L., M.A.L., E.C.C., and G.C. were responsible for the conceptualisation and methodology of the study. The investigation was conducted by S.L. The design and development of the prototype, interface, and control architecture were carried out by S.L. The writing and preparation of the original draft were undertaken by S.L., while M.A.L., E.C.C., and G.C. reviewed and revised the text. Supervision was provided by M.A.L., E.C.C., and G.C. All authors have read and approved the final version of the manuscript.

Financial support. This work was supported by funding from the Pprime Institute (UPR 3346) for the development of the prototype.

Competing interests. The authors declare that no conflicts of interest exist.

Ethical approval. Not applicable.

References

[1] World Health Organization. (2015). World report on ageing and health. World Health Organization. Accessed: 2024-09-19.
[2] Eurostat, Demographic structure and population aging, (2020). Accessed: 2024-09-19.
[3] S. Leone, L. Giunta, V. Rino, S. Mellace, A. Sozzi, F. Lago, E. M. Curcio, D. Pisla and G. Carbone, "Design of a wheelchair-mounted robotic arm for feeding assistance of upper-limb impaired patients," *Robotics* **13**(3), 38 (2024).
[4] European Agency for Safety and Health at Work (EU-OSHA), *Work-Related Musculoskeletal Disorders - Facts and Figures* (Publications Office of the European Union, Luxembourg, 2020).
[5] K. Moulaei, K. Bahaadinbeigy, A. A. Haghdoostd, M. S. Nezhad and A. Sheikhtaheri, "Overview of the role of robots in upper limb disabilities rehabilitation: A scoping review," *Arch. Public Health* **81**(1), 84 (2023).
[6] R. Trochimczuk, T. Huścio, S. Grymek and D. Szalewska, "Rehabilitation device supporting active and passive upper limb exercises," *Curr. Sci.* **115**(5), 868–873 (2018).
[7] B. Brahmi, M. Saad, C. O. Luna, P. S. Archambault, and M. H. Rahman, "Passive and active rehabilitation control of human upper-limb exoskeleton robot with dynamic uncertainties," *Robotica* **36**(11), 1757–1779 (2018).
[8] S. Leone, M. A. Laribi, E. Castillo-Castañeda and G. Carbone, "An Interactive Combined Mechatronic Approach to Enhance Upper Limb Rehabilitation," **In:** *Advances in Italian Mechanism Science* (Springer Nature Switzerland, Cham, 2024) pp. 19–26.
[9] R. Fareh, A. Elsabe, M. Baziyad, T. Kawser, B. Brahmi and M. H. Rahman, "Will your next therapist be a robot?-a review of the advancements in robotic upper extremity rehabilitation," *Sensors (Basel)* **23**(11), 5054 (2023).
[10] M. Perrelli, F. Lago, S. Garofalo, L. Bruno, D. Mundo and G. Carbone, "A critical review and systematic design approach for innovative upper-limb rehabilitation devices," *Robot. Auton. Syst.* **183**, 104835 (2025).
[11] D. M. Mahfouz, O. M. Shehata, E. I. Morgan and F. Arrichiello, "A comprehensive review of control challenges and methods in end-effector upper-limb rehabilitation robots," *Robotics* **13**(12), 181 (2024).
[12] H. Jin, M. Luo, S. Lu, Q. He and Y. Lin, "Design and Analysis of a Novel Variable Stiffness Joint for Robot," **In:** *Actuators* (Vol. 12, No. 1, MDPI, 2022) p. 10.
[13] N.-D. Vuong, R. Li, C.-M. Chew, A. Jafari and J. Polden, "A novel variable stiffness mechanism with linear spring characteristic for machining operations," *Robotica* **35**(7), 1627–1637 (2017).
[14] W. Wang, X. Fu, Y. Li and C. Yun, "Design and implementation of a variable stiffness actuator based on flexible gear rack mechanism," *Robotica* **36**(3), 448–462 (2018).
[15] M. Zhang, P. Ma, F. Sun, X. Sun, F. Xu, J. Jin and L. Fang, "Dynamic modeling and control of antagonistic variable stiffness joint actuator," *Actuators* **10**(6), 116 (2021).
[16] Z. Li and S. Bai, "A novel revolute joint of variable stiffness with reconfigurability," *Mech. Mach. Theory* **133**, 720–736 (2019).
[17] A. Firouzeh, M. Salerno and J. Paik, "Stiffness control with shape memory polymer in underactuated robotic origamis," *IEEE Trans. Robot.* **33**(4), 765–777 (2017).
[18] M. Cianchetti, C. Laschi, A. Menciassi and P. Dario, "Biomedical applications of soft robotics," *Nat. Rev. Mater.* **3**(6), 143–153 (2018).

https://doi.org/10.1017/S0263574725102671 Published online by Cambridge University Press

[19] S. Rodinò, E. M. Curcio, E. Sgambitterra and C. Maletta, "SMA-Polymer composite made by 3D printing: Modelling and experiments," *Procedia Structural Integrity* **47**, 579–588 (2023). 27th International Conference on Fracture and Structural Integrity (IGF27).
[20] T. Atakuru, G. Züngör and E. Samur, "Layer jamming of magnetorheological elastomers for variable stiffness in soft robots," *Exp. Mech.* **64**(3), 393–404 (2024).
[21] J. Choi, D.-Y. Lee, J.-H. Eo, Y.-J. Park and K.-J. Cho, "Tendon-driven jamming mechanism for configurable variable stiffness," *Soft Robot.* **8**(1), 109–118 (2021).
[22] M. Baggetta, G. Berselli, G. Palli and C. Melchiorri, "Design, modeling, and control of a variable stiffness elbow joint," *Int. J. Adv. Manuf. Technol.* **122**(11-12), 4437–4451 (2022).
[23] M. G. Contreras-Calderón, E. Castillo-Castañeda and M. A. Laribi, "Integration of variable stiffness actuators in a five-bar device to assist in active rehabilitation of the arm," *Meccanica* **57**(3), 697–706 (2022).
[24] D. P. Allen, E. Bolívar, S. Farmer, W. Voit and R. D. Gregg, "Mechanical simplification of variable-stiffness actuators using dielectric elastomer transducers," *Actuators* **8**(2), 44 (2019).
[25] Y. Liu, S. Cui and Y. Sun, "Mechanical design and analysis of a novel variable stiffness actuator with symmetrical pivot adjustment," *Front. Mech. Eng.* **16**(4), 711–725 (2021).
[26] M. Harder, M. Keppler, X. Meng, C. Ott, H. Höppner and A. Dietrich, "Simultaneous motion tracking and joint stiffness control of bidirectional antagonistic variable-stiffness actuators," *IEEE Robot. Autom. Let.* **7**(3), 6614–6621 (2022).
[27] L. Zongxing, L. Wanxin and Z. Liping, "Research development of soft manipulator: A review," *Adv. Mech. Eng.* **12**(8), 1687814020950094 (2020).
[28] B. A. Neibling, S. M. Jackson, K. S. Hayward and R. N. Barker, "Perseverance with technology-facilitated home-based upper limb practice after stroke: A systematic mixed studies review," *J. Neuroeng. Rehabil.* **18**(1), 43 (2021).
[29] S. Di, W. Zhang, W. Zhang and X. Ding, "A review on lower limb rehabilitation exoskeleton robots," *Chin. J. Mech. Eng.* **32**(1), 74 (2019).
[30] J. Narayan, B. Kalita and S. K. Dwivedy, "Development of robot-based upper limb devices for rehabilitation purposes: A systematic review," *Augment. Hum. Res.* **6**(1), 4 (2021).
[31] A. Olczak, A. Truszczyńska-Baszak and A. Stępień, "The use of Armeo® Spring device to assess the effect of trunk stabilization exercises on the functional capabilities of the upper limb—An observational study of patients after stroke," *Sensors* **22**(12), 4336 (2022).
[32] T. Proietti, E. Ambrosini, A. Pedrocchi and S. Micera, "Wearable robotics for impaired upper-limb assistance and rehabilitation: State of the art and future perspectives," *Ieee Access* **10**, 106117–106134 (2022).
[33] T. Takebayashi, K. Takahashi, S. Amano, Y. Uchiyama, M. Gosho, K. Domen and K. Hachisuka, "Assessment of the efficacy of ReoGo-J robotic training against other rehabilitation therapies for upper-limb hemiplegia after stroke: Protocol for a randomized controlled trial," *Front. Neurol.* **9**, 730 (2018).
[34] S. Monteleone, F. Negrello, M. G. Catalano, M. Garabini and G. Grioli, "Damping in compliant actuation: A review," *IEEE Robot. Autom. Mag.* **29**(3), 47–66 (2022).
[35] A. Garzo, J. H. Jung, J. Arcas-Ruiz-Ruano, J. C. Perry and T. Keller, "Armassist: A telerehabilitation solution for upper-limb rehabilitation at home," *IEEE Robot. Autom. Mag.* **30**(1), 62–71 (2022).
[36] M. G. Contreras-Calderón, J. Sandoval, M. Arsicault, E. Castillo-Castañeda and M. A. Laribi, "Experimental Validation of a Variable Stiffness Joint with Antagonistic Springs," **In:** *New Advances in Mechanisms, Transmissions and Applications* (M. A. Laribi, C. A. Nelson, M. Ceccarelli and S Zeghloul, eds.) Springer Nature Switzerland, Cham, 2023) pp. 23–31.
[37] M. G. Contreras-Calderón, M. A. Laribi, M. Arsicault and E. Castillo-Castañeda, "Design, analysis, and simulation of a new variable stiffness joint based on antagonist principle," *Proceedings of the Institution of Mechanical Engineers, Part C: Journal of Mechanical Engineering Science* **236**(18), 9991–10000 (2022).
[38] I. Wang, S.-C. Yen, M. Rahman, X. Li, E. Longwell-Grice and C.-J. Liu, "Hierarchical properties and functional staging of the Fugl-Meyer assessment lower extremity scale," *Arch. Phys. Med. Rehab.* **103**(12), e114 (2022).

Cite this article: S. Leone, M. A. Laribi, E. Castillo-Castaneda and G. Carbone (2025). "Interactive mechatronic system for improving upper limb rehabilitation", Robotica **43**, 3755–3781. https://doi.org/10.1017/S0263574725102671

https://doi.org/10.1017/S0263574725102671 Published online by Cambridge University Press